Published in final edited form as:
*ACS Chem Biol*. 2013 July 19; 8(7): 1567–1575. doi:10.1021/cb400170b.

# Quantification of cellular poly(ADP-ribosyl)ation by stable isotope dilution mass spectrometry reveals tissue- and drug-dependent stress response dynamics

**Rita Martello**[1,2,5], **Aswin Mangerich**[1,3,5,*], **Sabine Sass**[1], **Peter C. Dedon**[3,4], and **Alexander Bürkle**[1,*]

[1]Molecular Toxicology Group, University of Konstanz, Konstanz, 78464, Germany

[2]Konstanz Research School Chemical Biology, University of Konstanz, Konstanz, 78464, Germany

[3]Department of Biological Engineering, Massachusetts Institute of Technology, MA, 02193, Cambridge, USA

[4]Center for Environmental Health Science, Massachusetts Institute of Technology, MA, 02193, Cambridge, USA

## Abstract

Poly(ADP-ribosyl)ation is an essential posttranslational modification with the biopolymer poly(ADP-ribose) (PAR). The reaction is catalyzed by poly(ADP-ribose) polymerases (PARPs) and plays key roles in cellular physiology and stress response. PARP inhibitors are currently being tested in clinical cancer treatment, in combination therapy, or as monotherapeutic agents by inducing synthetic lethality. We have developed an accurate and sensitive bioanalytical platform based on isotope dilution mass spectrometry in order to quantify steady-state and stress-induced PAR levels in cells and tissues and to characterize pharmacological properties of PARP inhibitors. In contrast to existing PAR-detection techniques, the LC-MS/MS method uses authentic isotope-labeled standards, which provide unequivocal chemical specificity to quantify cellular PAR in absolute terms with femtomol sensitivity. Using this platform we analyzed steady-state levels as well as stress-induced dynamics of poly(ADP-ribosyl)ation in a series of biological systems including cancer cell lines, mouse tissues, and primary human lymphocytes. Our results demonstrate a rapid and transient stress-induced increase in PAR levels by >100-fold in a dose- and time-dependent manner with significant differences between cell types and individual human lymphocyte donors. Furthermore, *ex vivo* pharmacodynamic studies in human lymphocytes provide new insight into pharmacological properties of clinically relevant PARP inhibitors. Finally, we adapted the LC-MS/MS method to quantify poly(ADP-ribosyl)ation in solid tissues and identified tissue-dependent associations between PARP1 expression and PAR levels in a series of different mouse organs. In conclusion, this study demonstrates that mass spectrometric quantification of cellular poly(ADP-ribosyl)ation has a wide range of applications in basic research as well as in drug development.

[*]To whom correspondence should be addressed: A.M. Tel: 0049-7531-88-4067; Fax: 49-(0)7531-88-4033; aswin.mangerich@uni-konstanz.de or A.B. Tel: 0049-7531-88-4035; Fax: 49-(0)7531-88-4033; alexander.buerkle@uni-konstanz.de.
[5]These authors contributed equally to this work

**ASSOCIATED CONTENT**

Supporting Information Available: This material is available free of charge via the Internet (http://pubs.acs.org/journal/acbcct)

## INTRODUCTION

Poly(ADP-ribosyl)ation (PARylation) is a multifaceted post-translational modification that plays key roles in cellular physiology and genotoxic stress response (1, 2). Given the importance of PARylation in cell function, numerous approaches have been developed to characterize and quantify the polymeric modification, yet all suffer from inherent limitations. Here we describe a novel mass spectrometry platform that overcomes these problems and we applied this to a series of biological systems to characterize cellular PARylation.

PARylation mainly takes place in the nucleus and to a lesser extent also in the cytoplasm (1–3). The reaction is carried out by poly(ADP-ribose) polymerases (PARPs, also named ARTDs (4)) that use $NAD^+$ to synthesize poly(ADP-ribose) (PAR) with variable branching and chain length of up to 200 ADP-ribose units (Figure 1) (4). With nucleic acid-like properties, PAR differs from DNA and RNA by the presence of 1′–2″ ribose-ribose glycosidic linkages, 5′–5″ pyrophosphate linkages and branching with ADP-ribose moieties linked by 1‴–2″ ribose-ribose glycosidic bonds (2, 5). PARylation occurs in a covalent manner by modifying specific amino acids or non-covalently via distinct PAR binding motifs (1, 2, 4, 6). Thereby, it modulates physico-chemical properties of target proteins, including histones and PARPs themselves (automodification). Of note, stress-induced PARylation is transient, since PAR is rapidly hydrolyzed by poly(ADP-ribose) glycohydrolase (PARG) (7). Of the 17 human *PARP* gene family members, PARP1 contributes to ~90% of the cellular PAR synthesis upon induction of genotoxic stress (1, 8–12). DNA-damage-dependent PARylation has pleiotropic functions in genome maintenance, including DNA repair (1), telomere length regulation (13, 14) and re-initiation of stalled replication forks (15). In addition, it is involved in a host of cell functions, such as chromatin remodeling (16), transcription (17), signaling (18–20), cell cycle (18), apoptosis (19), and epigenetics (16). These functions link PARylation to mechanisms of inflammation and metabolism (21), as well as tumor suppression and longevity assurance, for which PARP inhibitors are currently clinically evaluated in tumor therapy (1, 22–25).

Given the significance of PARylation in biomolecular research and pharmaceutical drug development, its accurate and reliable quantification is essential for investigating its complex role on a cellular and organismic level. However, in particular the quantitative analysis of basal PAR levels in cells is a challenging task that requires analyte-specific, highly sensitive methods. Early techniques to study cellular PAR levels used dihydroxyboryl-biorex (DHBB) affinity chromatography to isolate PAR (26–29), which was followed by compound derivatization and LC-based detection. These techniques, first developed by Jacobson et al. (26), allowed accurate quantification, however routine usage was hampered by the amount of cellular material required, radioactive labeling or derivatization of the analytes, and by the overall time-consuming procedure. Other approaches were based on treating cells with radioactively-labeled PAR precursors such as adenine (29, 30). Although leading to precise results, these techniques were prone to overestimate PAR levels, due to artificial DNA damage induced by the radioactive isotopes and subsequent collateral PARP activation. Most current tools to quantify PAR rely on antibodies, which due to their convenience are widely used in basic research as well as preclinical and clinical studies (31, 32). However, such approaches are limited with regards to sensitivity and linearity of quantification. For example, one of the most widely used anti-PAR antibody, *i.e.*, 10H, prefers binding to long PAR chains over short ones, thus leading to a potential underestimation of PAR levels and lack of linearity in quantification (33, 34). Furthermore, immuno-based methods lack chemical specificity and do not use internal standards to control for losses during sample preparation.

Isotope dilution mass spectrometry is the current gold standard to quantify nucleosides derived from DNA and RNA, including enzymatic modifications and damage products (35, 36), but corresponding methods to quantify cellular PAR have so far not been described. To overcome the limitations of earlier PAR quantification methods, we developed an HPLC-coupled tandem mass spectrometric (LC-MS/MS) platform to robustly and accurately quantify PARylation in cells and tissues in absolute terms with formerly unmet sensitivity and chemical specificity. Using this method we determine PAR levels in various biological systems revealing cell type- and tissue-specific differences in PARylation dynamics. Furthermore, *ex vivo* pharmacodynamic studies in human lymphocytes using clinically relevant PARP inhibitors demonstrate that this method has a wide range of applications in basic research as well as pharmaceutical drug development.

## RESULTS AND DISCUSSION

### An LC-MS/MS-based platform for quantifying cellular PAR

We developed a highly sensitive and precise method to quantify cellular PARylation based on isotope dilution mass spectrometry. To optimize reproducibility, sensitivity, and specificity of PAR quantification and to enhance sample throughput, the LC-MS/MS-based method implements several important innovations compared to previous approaches (26): First, stable-isotope-labeled PAR was synthesized and used as an authentic internal standard; second, commercially available RNA isolation kits were adapted to extract PAR from cells and tissues in a standardized, routine manner; third, characteristic PAR-derived nucleosides were generated by enzymatic digestion and separated chromatographically; and fourth, these products were quantified by means of tandem mass spectrometry. The overall method workflow comprises four key steps that can be accomplished in about two days (Figure 1): (i) precipitation of all cellular macromolecules by trichloroacetic acid (TCA) and addition of the internal standard; (ii) detachment of protein-bound PAR by alkaline treatment and removal of DNA, RNA, and proteins by enzymatic digestion; (iii) PAR extraction either by solid-phase extraction or DHBB affinity chromatography; and (iv) enzymatic digestion of PAR to individual characteristic nucleosides and mass spectrometric analysis.

**i.** To achieve the most rigorous quantification possible, after TCA precipitation of cellular macromolecules, $^{13}C,^{15}N$-labeled PAR was added in defined amounts to each sample as an authentic chemical standard. This approach ensures unequivocal chemical specificity for the analyte and minimizes technical variability of the method. Since $^{13}C,^{15}N$-labeled PAR is not commercially available and its synthesis has not been described before, we developed a one-step *in vitro* protocol for the synthesis of $^{13}C,^{15}N$-labeled PAR (Figure S1). This reaction is based on the use of rec. NMNAT1 which converts $^{13}C,^{15}N$-labeled ATP and non-labeled nicotinamide mononucleotide (NMN) to $^{13}C,^{15}N$-labeled $NAD^+$. This serves as a substrate for rec. PARP1 to synthesize $^{13}C,^{15}N$-labeled PAR. The quality and nature of labeled PAR was validated using the anti-PAR-specific monoclonal antibody (mAB) 10H in combination with LC-MS/MS characterization (Figure S1C).

**ii.** In TCA-precipitated material, PAR was quantitatively detached from proteins by alkaline treatment, which also converts monomeric protein-bound ADP-ribose to 5′-AMP, rendering this method specific for PAR. Thereafter, DNA, RNA and proteins were digested by DNase, RNase and proteinase K, respectively, which served as a means to reduce the complexity of the sample, since, if present in large excess compared to PAR, these macromolecules may interfere with PAR purification efficacy and LC-MS/MS quantification. Proteinase K digestion also served as a second means to ensure the formation of protein-free PAR molecules.

iii. Next, PAR was extracted via solid-phase extraction or DHBB-affinity chromatography. The latter is the classical method to selectively extract cellular PAR (30, 37), but this method has some limitations and is not suited for routine analyses, due to the variability in the quality of the prepared DHBB batches, the large volumes used for washing and elution, and the overall time-consuming procedure. To overcome these hurdles, we reasoned that RNA isolation methods may be suitable of PAR extraction, given the similar chemical structure of the building blocks of PAR and RNA. Therefore, we tested a set of commercially available RNA extraction kits and compared those to classical DHBB chromatography and phenol/chloroform extraction. Two RNA extraction kits, *i.e.*, the Roche High pure microRNA isolation kit (R) and the PeqLab PeqGold RNA pure kit (PL) led to a high recovery of PAR in terms of quantity and quality, *i.e.*, no loss of overall PAR signal and no bias in the extraction efficacy of PAR of different chain length was observed (Figure S2A). To test if these methods can be used to extract cellular PAR, untreated or $H_2O_2$-treated COPF5 cells were subjected to the different purification methods. Using immuno-slot blotting, basal PAR levels from untreated cells were below the limit of detection in $1 \times 10^7$ cells (Figure 2A), but a PAR-derived signal was detected in $H_2O_2$-stimulated cells with all extraction methods used. Except for phenol/chloroform extraction, all other extraction methods demonstrated efficient recovery rates, with the strongest signal detected with kit R (Figure 2B).

iv. Since PAR is highly variable in chain length, it was hydrolyzed to characteristic monomeric nucleosides using phosphodiesterase (PDE) and alkaline phosphatase (AP) prior to LC-MS/MS analysis (Figure S2B). Digestion products include adenosine (Ado), ribosyladenosine (R-Ado), and diribosyladenosine ($R_2$-Ado), which are characteristic of the terminal, linear, or branched part of the polymer, respectively. Whereas R-Ado and $R_2$-Ado are diagnostic for PAR, Ado is not, since it can also be derived from cellular RNA. Samples were subjected to HPLC to reduce the complexity of the sample, and hence to enhance sensitivity of the subsequent mass spectrometric quantification. This method permits baseline separation of all expected PAR-digestion products within a runtime of 20 min (Figure 1B). Since cellular PAR consists >98–99% of R-Ado (see references (27, 28) and Figure 4C), we focused on this analyte for quantification. Daughter ion scans of R-Ado (m/z of 400) revealed that after collision-induced fragmentation the most prevalent ion represents adenine (m/z of 136) (Figure S3A). Therefore the transitions of m/z 400 $\rightarrow$ 136 and m/z 415 $\rightarrow$ 146 were monitored for the quantification of unlabeled and $^{13}C/^{15}N$-labeled R-Ado, respectively. The limits of quantification for R-Ado were <50 fmol on different LC-MS/MS systems used. We quantified the cellular PAR referring to the area ratio of unlabeled R-Ado to $^{13}C,^{15}N$-labeled R-Ado. Usually we observed a recovery rate of $^{13}C,^{15}N$-labeled R-Ado of 50–60% which is comparable to other techniques. Absolute PAR values were then calculated by means of calibration curves (Figure S3B). These were acquired on a daily basis using unlabeled and $^{13}C/^{15}N$-labeled R-Ado standards, which were purified from *in-vitro*-synthesized PAR (Figure S3C).

## Characterization of cellular PARylation dynamics

Three different cell types, *i.e.*, COPF5 cells, HeLa cells, and primary human PBMCs, were used to validate the method in terms of sensitivity, robustness and performance in comparison with immuno-based PAR detection techniques. These results revealed cell-type-specific characteristics of toxicant-induced PARylation dynamics.

LC-MS/MS analysis of PAR extracted from COPF5 cells confirmed results by immuno-slot blotting, demonstrating that DHBB-chromatography as well as kit R yielded comparable recovery rates of PAR (Figure 2B and C). Next, we analyzed PARylation in a clinically relevant cell type; to this end, we isolated PBMCs from fresh blood of healthy volunteers. Using LC-MS/MS-based quantification, it was possible to determine basal PAR levels above the limit of quantification in <10 million unstimulated PBMCs, which corresponds <10 ml of whole blood (Figure 2D). The absolute R-Ado levels were in the range of 0.02 – 0.06 amol/cell and increased by >50-fold in $H_2O_2$-treated PBMCs (Figure 2D–F). Assuming an average chain length of 10 ADP-ribose units per PAR molecule ($PAR_{10mer}$), this corresponds to about 3,000 $PAR_{10mer}$ molecules under physiological conditions and >150,000 molecules upon induction of genotoxic stress. Notably, these results are in full accordance with published values in different cell types using earlier techniques (26), demonstrating the reliability of our method.

To assess robustness and reproducibility of the method, independent experiments were performed on separate days using PBMCs from the same donor. As is evident from Figure 2E, $H_2O_2$ treatment resulted in a highly significant induction of PAR levels with standard deviations of <11% and <16% for untreated and $H_2O_2$-treated cells, respectively. Interestingly, when analyzing PAR levels in PBMCs from different donors, to assess biological inter-donor variability, it became apparent that basal PAR levels show little variation between donors, ranging from 0.02 – 0.06 amol/cell. In contrast, $H_2O_2$-induced levels displayed considerable inter-donor variation, ranging from ~1 to >10 amol/cell, which corresponds to an induction level of 20 – 300-fold (Figure 2F). These results point to considerable heterogeneity in the stress-induced PARylation response in the human population.

Next, we evaluated the sensitivity and quantitative range of our method by comparing it with immuno-based epifluorescence microscopy (IF) in HeLa cells, which is widely used to evaluate relative differences in PARylation on a single cell level (31). Using IF, we did not detect PAR-derived signals above background in untreated cells (Figure 3). In contrast, LC-MS/MS analysis yielded R-Ado peaks above the limit of quantification using 5 million untreated cells, which corresponds to one subconfluent 10-cm petri dish, with levels ranging from 0.05 – 0.1 amol/cell (Figure 3B). Both methods demonstrated an increase in PAR-derived signals in cells treated with increasing doses of $H_2O_2$. However, while IF-based analysis detected increases of PAR-derived signals above background at 100 μM $H_2O_2$ (Figure 3), the LC-MS/MS method revealed a trend for PARP induction already at an $H_2O_2$ concentration of 10 μM which reached statistical significance at 50 μM (Figure 3B). These results indicate that the LC-MS/MS method is able to detect cellular PAR with much higher sensitivity compared to classical IF, even under physiological conditions and upon induction of mild genotoxic stress. The detection of basal PAR levels is achievable in a convenient number of cells, *i.e.*, <5–10 million cells depending on cell type, which corresponds to one subconfluent 10-cm petri dish of adherent cells in culture or 10 ml human blood.

To analyze DNA-damage-induced PARylation dynamics, we performed dose-response and time-course experiments in COPF5 cells and PBMCs. Whereas basal PAR levels in COPF5 cells were in the same range as observed for PBMCs and HeLa cells, *i.e.*, 0.02 – 0.13 amol/cell, cell-type-specific responses became evident upon induction of DNA damage. Thus, after treating cells for 5 min with 100 μM $H_2O_2$, COPF5 cells displayed a 16-fold increase in PAR levels, whereas PBMCs isolated from a single donor on different days showed a 53-fold increase in PAR levels (Figure 4A). The lower induction levels of PARylation in COPF5 cells compared to PBMCs and HeLa cells could either originate from more efficient antioxidant defense systems in COPF5 cells or differences in PARP regulatory mechanisms. Time-course experiments revealed a cell-type specific, highly dynamic and transient nature

of PARylation in COPF5 cells and PBMCs upon induction of DNA damage. Thus, $H_2O_2$ treatment resulted in peak levels of PAR after 2.5 min and 10 min in PBMCs and COPF5 cells, respectively (Figure 4B). Thereafter, PAR levels declined rapidly most likely due to PARG activity. Whereas levels decreased nearly to background levels already after 15 min in PBMCs, in COPF5 cells 30% of maximum PAR levels were still detectable 30 min after $H_2O_2$ treatment. In conclusion, these results indicate that the LC-MS/MS method can serve as a diagnostic tool to monitor the impact of genotoxic exposure or treatment on human tissue (e.g., PBMC or tumor tissue). Furthermore, the finding that different cell types and PBMCs from different donors show considerable variability in PARylation dynamics could be of fundamental importance with respect to the use of PARP inhibitors in cancer therapy, in particular, when applied in combination with DNA-damaging chemotherapeutics.

It is noteworthy that the digestion product $R_2$-Ado which is diagnostic for PAR branching points was also detected in $H_2O_2$-treated cells (Figure 4C **and** S3D). By comparing the area ratios of $R_2$-Ado to R-Ado, it can be estimated that the branching frequency of PAR was 1 – 2% in different cell types (Figure 4C), which is in accordance with previously published values (27). No dose-response relationship was observed for the $R_2$-Ado/R-Ado ratio, suggesting that dose-dependent increases in PAR levels arise from the formation of more PAR molecules rather than from increases in chain length. It should be stressed that these values give an estimate of PAR branching, since a completely confident determination of branching sites requires the purification of sufficient amounts of unlabeled and $^{13}C,^{15}N$-labeled $R_2$-Ado to acquire corresponding calibration curves. This requires large-scale, preparative PAR synthesis and subsequent HPLC purification of $R_2$-Ado.

## Using the LC-MS/MS method as a tool for cancer and PARylation research

PARP inhibitors are currently under clinical evaluation in cancer treatment either in combination with classical chemo- or radiotherapy, or as stand-alone drugs following the concept of synthetic lethality (1, 22–24). Based on our investigations in PBMCs, we tested, whether the LC-MS/MS method is suitable for analyzing the *ex vivo* efficacy of PARP inhibitors in a clinically relevant cell type. Therefore, we isolated PBMCs from healthy donors and incubated them with increasing concentrations of either of two PARP inhibitors currently in clinical evaluation, *i.e.*, ABT-888 or olaparib, prior to stimulation with $H_2O_2$ and LC-MS/MS analysis (Figure 5). Both compounds showed a similar dose-dependent inhibition of cellular PARylation with $IC_{50}$ values <1 μM. Notably, these values vary from those determined by PAR immunoassays (38), demonstrating that the detection of PAR with background sensitivity significantly influences the outcome of pharmacodynamic studies. Importantly, inhibitor-specific differences became apparent at higher inhibitor concentrations of 10 μM. In this case, we detected PAR levels of 0.4 to 0.9 amol/cell in cells preincubated ABT-888, which are above background levels of <0.1 amol/cell, whereas 10 μM olaparib almost completely suppressed $H_2O_2$-induced PARP activity to levels of 0.1 to 0.2 amol/cell.

LC-MS/MS-based techniques are widely used in pharmaceutical drug development based on their reliability, chemical specificity, and automation potential. PBMCs represent a valuable pharmacodynamic surrogate for tumor biopsies in clinical trials, because they are readily accessible, their collection is non-invasive, and they allow longitudinal evaluation of drug activity during therapeutic treatment schedules (38). Our findings that different cell types and PBMCs from different donors display substantial variability in PARylation dynamics suggest that measuring PARP activity may be useful to define dosing and timing of DNA-damaging chemotherapeutics, when used in combination with PARP inhibitors. In addition to the *ex vivo* pharmacodynamic studies as described here, the LC-MS/MS method can be extended for the analysis of PAR levels in solid tissues. *In vivo* measurements of PARP

activity can be important to identify patients that are susceptible to PARP inhibitor treatment. Furthermore, in human tumor biopsies, analysis of PARylation can be valuable to study drug bioavailability in the target organ by measuring its ability to inhibit PARP activity. As described in the following, our analysis of PARylation in mouse tissues lay the foundation of such studies (Figure 6).

The analysis of basal PAR levels is largely unexplored, but potentially of high relevance, as several groups report that PARylation is responsible for cellular functions also in the absence of genotoxic stress (1, 2, 4, 10, 17). To obtain first insight into the physiological significance of PARylation within the mammalian organism, we adapted the procedure to analyze PARylation in mouse tissues. To this end, tissues were harvested, disrupted in 10% TCA, and essentially processed as were cellular samples with slight modifications. As cell numbers are not available for tissue samples, an important modification represents the normalization of the mass-spectrometric R-Ado signal to the tissue DNA content. Therefore, the DNA content of each sample was determined using a fluorescence-spectrophotometric method based on the usage of the DNA binding dye Hoechst 33342 (Figure S4A). This normalization method provided reproducible results within a range of tissue amounts typically subjected to analysis (50 to 200 mg) (Figure S4B). To induce tissue PAR formation we irradiated freshly harvested spleen and liver samples *ex vivo* using increasing doses of X-rays, which are able to penetrate the tissue, thereby inducing DNA strand breaks and oxidative base lesions. Liver and spleen both showed a dose-dependent induction of PAR formation (Figure 6A). Interestingly, basal PAR levels turned out to be ~2-fold lower in spleen compared to liver. However, whereas PAR formation was induced only by ~4 fold in liver upon high-dose X-ray irradiation, PAR levels were observed to be ~20-fold higher in irradiated spleens compared to untreated samples. Notably, screening of 7 different mouse organs revealed R-Ado levels above the limit of quantification in all organs analyzed (Figure 6B). To our knowledge this is the first comparative analysis reporting PAR levels in a spectrum of different mouse tissues. Substantial differences in basal PAR levels were detected in these tissues, e.g., revealing ~10-fold higher PAR levels in heart as compared to lung tissue. Interestingly, organs with moderate PARP1 expression levels, such as lung, liver, kidney and heart, displayed a strong positive correlation between PARP1 expression and basal PAR levels, pointing to tissue-dependent associations between PARP1 expression and poly(ADP-ribosylation) levels. In contrast, organs with high PARP1expression levels, such as spleen, thymus, and testis, showed low basal levels of cellular PAR (Figure 6C). This may be related to stringent regulatory mechanisms to control PARP activity, such as posttranslational modifications of PARPs, intracellular $NAD^+$ levels, or PARG activity. In general this suggests that basal PAR levels may play significant roles in normal tissue function.

In conclusion, PARylation is emerging as a ubiquitous post-translational protein modification with central functions on a cellular and organismic level. We have developed and applied an LC-MS/MS-based bioanalytical platform for absolute quantification of steady-state and stress-induced PAR levels in cells and tissues, which overcomes several limitations commonly encountered in PAR quantification. By using isotope dilution mass spectrometry, our method shows improved chemical specificity and sensitivity compared to previous methods (26–29, 31, 32). Furthermore, our protocol ensures quick and reliable sample preparation, which allows screening of multiple samples in parallel. Thereby, this approach combines the accuracy and precision of a chemical, bioanalytical technique with the convenience of a standardized, routine method. As demonstrated by analyzing PARylation dynamics in cancer cell lines and human PBMCs as well as characterizing pharmacological properties of PARP inhibitors, the LC-MS/MS platform represents a valuable tool to facilitate our understanding on PARylation metabolism during physiological and pathophysiological conditions.

# METHODS

## Antibodies and recombinant proteins

The anti-PAR specific mouse monoclonal antibody 10H was immuno-purified on a protein A column (Sigma-Aldrich) from hybridoma cell culture supernatant as described previously (33). Recombinant (rec.) NMNAT1 was a gift from M. Ziegler (University of Bergen). Rec. hPARP1 was overexpressed in *Sf*9 cells using the baculovirus system and purified as described previously (39, 40).

## *IN VITRO* synthesis of PAR

$^{13}C,^{15}N$-labeled PAR was synthesized in a 140 μl reaction mixture containing 60 mM HEPES (pH 7.4), 7 mM $MgCl_2$, 1.2 mM $^{13}C^{15}N$-labeled ATP (B.A.C.H. UG), 1.2 mM nicotinamide mononucleotide (NMN), 4 mM DTT, 60 μg/ml histone H1, 60 μg/ml histone HIIa, 50 μg/ml octameric oligonucleotide GGAATTCC (Life Technologies), $3.8 \times 10^{-2}$ U/ml NMNAT1, and 150 nM hPARP1. After incubation at 37° C for 1 h, the reaction was stopped by adding 1 ml ice-cold 20% TCA (v/w) and $^{13}C,^{15}N$-labeled PAR was purified as described previously (34). The overall reaction efficacy was ~30%. HPLC analysis was performed using a Hydro-RP column 80A 250 × 4.6 mm particle size 4 micron (Phenomenex) heated at 25 °C. For gradients details see Table S1. Unlabeled PAR was synthesized and purified as described previously (34).

## Monitoring of $NAD^+$ formation

Formation of $NAD^+$ was monitored by HPLC as described previously (41) with some modifications. Briefly, the reaction containing 60 mM HEPES (pH 7.4), 7 mM $MgCl_2$, 1.2 mM ATP, 1.2 mM NMN, $1.1 \times 10^{-2} - 1.1 \times 10^{-1}$ U/ml NMNAT1, 4 mM DTT was stopped by adding 50 μl ice-cold 1.2 M $HClO_4$. After incubation on ice for 10 min, samples were centrifuged for 1 min at 16000 × *g*: The supernatant was neutralized by adding 35 μl of 1 M $K_2CO_3$. Samples were incubated on ice for 15 min and centrifuged for 1 min at 16000 × *g*. To remove enzymes, the supernatant was filtered through a 10 kDa cutoff filter (nanosep 10K, Pall). Samples were snap-frozen in liquid nitrogen and stored at −80° until further usage. For HPLC analysis, samples were diluted 1:10 and injected into a Hydro-RP column 80A 250 × 4.6 mm particle size 4 micron (Phenomenex) heated at 25 °C. For gradients details see Table S1.

## Cells culture

HeLa S3 cells were grown in DMEM supplemented with 100 U/ml penicillin, 0.1 mg/ml streptomycin (Life Technologies), and 10% FCS (Biochrom) at 37°C, 95% humidity and 5% $CO_2$. COPF5 cells were additionally supplemented with 0.8 mg/ml G418 (PAA) for transgene selection. To isolate human PBMCs, peripheral venous blood was collected in citrate S-Monovettes (Sarstedt) from healthy 20–55-year-old donors. All experiments were conducted in accordance with the Declaration of Helsinki and ethical clearance was obtained from the University of Konstanz Ethics Committee. Aliquots of 10 ml of blood were diluted in 10 ml PBS [137 mM NaCl, 3 mM $KH_2PO_4$, 10 mM $Na_2HPO_4$, (pH 7.4)]. Thereafter, the solution was gently placed on top of 15 ml of Biocoll (Biochrom) in a 50-ml conical tube and centrifuged without brake at 800 × *g* and RT for 15 min. The recovered PBMCs were washed twice with PBS and cell numbers were determined using a CASY cell counter (Schärfe System). For the PARP inhibitor experiments, cells were pre-incubated with ABT-888 (Enzo Life Science) or olaparib (Selleckchem) for 30 min.

### Immuno-based PAR detection

Immunofluorescence analysis was carried out as described previously using MeOH/acetic acid (3:1) fixation (42). For immuno-slot-blot analysis, PAR extracted from COPF5 cells was vacuum aspirated onto a positively charged nylon membrane (Amersham Biosciences) using a slot-blot manifold (Schleicher & Schuell). After incubation at 90°C, the membrane was blocked with 5% (w/v) skim milk powder in 10 mM Tris-HCl (pH 8.0), 150 mM NaCl, and 0.05% (v/v) Tween 20 (TNT buffer). PAR was detected by incubating the membrane with monoclonal mouse-anti-PAR antibody (10H) diluted 1:300 in 5% (w/v) skim milk powder in TNT buffer for 1 h. Subsequently membranes were washed thrice in TNT buffer for 5 min and incubated for 1 h with peroxidase-conjugated anti-mouse IgG (DakoCytomation) diluted 1:2000 in 5% (w/v) skim milk in TNT buffer. Membranes were washed thrice for 5 min in TNT buffer and signals were visualized using the enhanced chemiluminescence reaction kit (GE Healthcare).

### Purification of cellular PAR

In the case of COPF5 and HeLa cells, medium was removed; cells were rinsed with PBS (pH 7.4), treated with or without $H_2O_2$ in PBS and incubated at 37°C. After removal of PBS, cells were harvested by addition of 2 ml 20% TCA (w/v) and the acid-insoluble material was detached from the dishes by scraping with a rubber policeman. TCA precipitation of PBMCs was performed by adding an equal volume of 20% TCA, followed by incubation on ice for 15 min. Subsequently, pellets were washed with ice-cold 70% ethanol, resuspended in 225 μl 0.5 M KOH, 50 mM EDTA and incubated at 37°C for 45 min. Alkaline treatment was stopped by adjusting the pH to 7 by drop-wise addition of 37% HCl. Alternatively samples can be neutralized by adding 50 μl MOPS buffer (4.8 M, pH 5.9). Afterwards, 5 pmol of $^{13}C$,$^{15}N$ labeled-PAR were added. DNA and RNA present in samples were digested by addition of 44 mM $MgCl_2$, 0.5 mM $CaCl_2$, 0.1 mg/ml DNAse I (Roche) and 55 μg/ml RNAse A (Sigma-Aldrich) at 37°C for 3 hours, following digestion with 0.2 mg/ml proteinase K (Roche) overnight.

The synthesis of the DHBB resin and PAR purification via DHBB chromatography was essentially carried out as described previously (30, 43), with modifications. Briefly, the suspension was prepared by dissolving 50 g of BioRex 70 (100–200 mesh) (Bio-Rad) in 300 ml $H_2O$ and allowed to swell for 30 min. Subsequently, water was aspirated through a glass filter, the resin was washed with 3 l $H_2O$ by filtration and then resuspended in 250 ml $H_2O$. pH was adjusted to 5.0 using 37% HCl followed by the addition of 5 g N-(3-dimethylaminopropyl)-N′-ethylcarbodiimide hydrochloride and the suspension was stirred at RT for 15 min. Thereafter, a solution consisting of 5 g of 3-aminophenyl boronic acid dissolved in 32 ml $H_2O$ was added, pH was adjusted to 5.0, and the suspension was stirred overnight in darkness. Next, the DHBB material was filtered through a glass filter and washed with 3 l $H_2O$, 3 l of 0.1 M NaAc, 1 M NaCl (pH 4.5), 3 l of 0.1 M $NaHCO_3$1 M NaCl (pH 9.0), 2.5 l $H_2O$ and 100 ml 6 M guanidine•HCl, 50 mM MOPS, 10 mM EDTA (pH 6.0). Finally, the DHBB resin was resuspended in an equal volume of 6 M guanidine•HCl, 50 mM MOPS, 10 mM EDTA pH 6.0 and stored at 4°C in darkness. DHBB affinity chromatography of PAR was carried out as described previously (30), with modifications. The DHBB suspension (2 ml) was centrifuged at 1000 × *g* for 5 min. The supernatant was removed and the resin was mixed with 6 ml of 6 M guanidine•HCl, 250 mM $NH_4Ac$ (pH 9.0). Following centrifugation, the DHBB material was washed twice with 7 ml $H_2O$ and once with 6 ml of 6 M guanidine•HCl, 250 mM $NH_4Ac$ (pH 9.0). Finally, the resin was resuspended in an equal volume of 6 M guanidine•HCl, 250 mM $NH_4Ac$ (pH 9.0). The PAR-containing TCA precipitate was resuspended in 1 ml of 6 M guanidine•HCl, 250 mM $NH_4Ac$, 10 mM EDTA (pH 6.0), followed by addition of 1 ml 0.5 M KOH, 50 mM EDTA and the solution was incubated at 37°C for 45 min. After the addition of 8 ml of 6 M

guanidine•HCl, 250 mM $NH_4Ac$ 10 mM EDTA, pH was adjusted to 9.0 using 37% HCl. The solution was incubated with 1 ml of the DHBB resin in a rotator at RT for 2 h in darkness. Thereafter, the suspension was poured into a PolyPrep chromatography column (Bio-Rad) and the flow-through was collected. The column was rinsed with 10 ml 6 M guanidine•HCl, 250 mM $NH_4Ac$ 10 mM EDTA (pH 9.0) and then washed with 10 ml of 1 M $NH_4HCO_3$, 10 mM EDTA (pH 9.0). Elution of PAR was performed twice with 5 ml $H_2O$. Samples were dialyzed twice against water by using dialysis cassettes 2000 MWCO (Pierce).

PAR extraction by phenol/chloroform extraction was carried out as described previously (34).

PAR extractions via the High pure miRNA isolation kit (Roche), PeqGOLD RNA pure (Peqlab), RNeasy kit (Qiagen) were performed analogous to the manufacturers' recommendations for the purification of RNA.

For PAR extraction from mouse organs, snap-frozen tissues were cut in pieces of ~2 mm and homogenized with a tissue disruptor Ultra-Turrax T25 (Janke & Kunkel) in 2 ml of 10% TCA (w/v). Precipitate was centrifuged at 3000 × *g* and 4°C for 10 min, washed twice with 70% EtOH and air-dried. Then pellets were resuspended in 400 μl 0.5 M KOH, 50 mM EDTA and incubated at 37 °C for 45 min. The cell debris was pelleted and supernatant was neutralized with 4.8 M MOPS (pH 5.9) and 30 μl aliquots were used for DNA concentration determination as described previously (44). Briefly, aliquots were neutralized with 2 M MOPS buffer and diluted in 180 μl dilution buffer (0.5 M KOH, 50 mM EDTA, 1 M MOPS). Standard curves using calf thymus DNA (Sigma-Aldrich) in concentrations from 0 ng/Ol to 150 ng/Ol were performed on a daily basis. To this end, standard solutions were denatured with 0.5 M KOH, 100 mM EDTA at 60° C for 1 h and neutralized 1:1 with 2 M MOPS buffer (pH 7). Standard solutions and samples were incubated for 5 min with 0.5 μg/ml Hoechst 33342 (Molecular Probes) and subsequently transferred into a 96-well plate in duplicates. The fluorescent measurements were carried out using a fluorescence reader FL600 (Biotek) with an excitation wavelength of 360/40 nm and an emission of 460/40 nm.

## Sample preparation and LC-MS/MS analysis

PAR was subjected to digestion with alkaline phosphatase from bovine intestine mucosa (AP) (Sigma-Aldrich) and phosphodiesterase I (PDE) (Affymetrix) before LC-MS/MS analysis. Samples were brought to a final volume of 500 μl in a solution containing 1 mM MgAc, 30 mM $NH_4Ac$, 10 U AP and 0.5 U PDE. Following incubation at 37°C for 3 h, the enzymes were removed using a 10 kDa cut-off filter (Nanosep 10K, Pall) by centrifugation at 14000 × *g* for 20 min. Cell extracts were vacuum-dried and resuspended in 100 μl of mobile phase prior to LC-MS/MS analysis. The digestion with AP and PDE was monitored by analyzing PAR on modified sequencing gels as described previously (34). To this end, samples were separated by 20% TBE-PAGE (500 mM Tris, 500 mM $H_3BO_3$, 10 mM EDTA) at 800 V and staining was carried out with Color Silver stain kit (Pierce) according to the manufacturer's instructions. Afterwards, HPLC separation of digestion products was performed using a Waters 2695 separation module and a Hypersil Gold aQ 150 × 2.1 mm particle size 3 micron (Thermo Scientific) at 30°C. Compounds were separated isocratically with 1% acetonitrile supplemented with 0.1% acetic acid at a flow rate of 0.3 ml/min. The column effluent was coupled to a Quattro Micro mass spectrometer (Waters) operating in positive ESI mode (for MS parameters see Table S2).

### HPLC purification of ribosyladenosine

Ribosyladenosine was purified from AP/PDE-digested *in-vitro*-synthesized PAR for usage as chemical standard (unlabeled and $^{13}C,^{15}N$-labeled). After digestion with AP and PDE and removing of enzymes by size-exclusion filtration (see above), digestion products were injected into the HPLC system (Waters 2695). The separation was carried out using a Hydro-RP column 80A 250 × 4.6 mm particle size 4 micron (Phenomenex) at 30 °C and a flow rate of 0.5 ml/min. PAR digestion products were eluted using a gradient protocol as detailed in Table S3.

## Supplementary Material

Refer to Web version on PubMed Central for supplementary material.

## Acknowledgments

We thank M. Ziegler (University of Bergen) for the kind gift of rec. NMNAT1, as well as A. Marx and M. Scheffner (University of Konstanz) for advice. We also thank M. Arsic for help in the initial phase of this study, H. Gerding, F. May, and A. Finke for contributions during their Bachelor projects, and P. Palombo for technical assistance. This work was funded by the *Deutsche Forschungsgemeinschaft (DFG)* through a KoRS-CB stipend to RM and through the CRC 969, and by the University of Konstanz. Funding was also provided by the US National Institutes of Health (grants ES002109, CA026731) and by the Singapore Alliance for Research and Technology.

## References

1. Rouleau M, Patel A, Hendzel MJ, Kaufmann SH, Poirier GG. PARP inhibition: PARP1 and beyond. Nat Rev Cancer. 2010; 10:293–301. [PubMed: 20200537]
2. Gibson BA, Kraus WL. New insights into the molecular and cellular functions of poly(ADP-ribose) and PARPs. Nat Rev Mol Cell Biol. 2012; 13:411–424. [PubMed: 22713970]
3. Leung AK, Vyas S, Rood JE, Bhutkar A, Sharp PA, Chang P. Poly(ADP-ribose) regulates stress responses and microRNA activity in the cytoplasm. Mol Cell. 2011; 42:489–499. [PubMed: 21596313]
4. Hottiger MO, Hassa PO, Luscher B, Schuler H, Koch-Nolte F. Toward a unified nomenclature for mammalian ADP-ribosyltransferases. Trends Biochem Sci. 2010; 35:208–219. [PubMed: 20106667]
5. Juarez-Salinas H, Mendoza-Alvarez H, Levi V, Jacobson MK, Jacobson EL. Simultaneous determination of linear and branched residues in poly(ADP-ribose). Anal Biochem. 1983; 131:410–418. [PubMed: 6311052]
6. Hakme A, Wong HK, Dantzer F, Schreiber V. The expanding field of poly(ADP-ribosyl)ation reactions 'Protein Modifications: Beyond the Usual Suspects' Review Series. EMBO Rep. 2008; 9:1094–1100. [PubMed: 18927583]
7. Min W, Wang ZQ. Poly (ADP-ribose) glycohydrolase (PARG) and its therapeutic potential. Front Biosci. 2009; 14:1619–1626.
8. Langelier MF, Planck JL, Roy S, Pascal JM. Structural basis for DNA damage-dependent poly(ADP-ribosyl)ation by human PARP-1. Science. 2012; 336:728–732. [PubMed: 22582261]
9. Ali AA, Timinszky G, Arribas-Bosacoma R, Kozlowski M, Hassa PO, Hassler M, Ladurner AG, Pearl LH, Oliver AW. The zinc-finger domains of PARP1 cooperate to recognize DNA strand breaks. Nat Struct Mol Biol. 2012; 19:685–692. [PubMed: 22683995]
10. Cohen-Armon M, Visochek L, Rozensal D, Kalal A, Geistrikh I, Klein R, Bendetz-Nezer S, Yao Z, Seger R. DNA-Independent PARP-1 Activation by Phosphorylated ERK2 Increases Elk1 Activity: A Link to Histone Acetylation. Mol Cell. 2007; 25:297–308. [PubMed: 17244536]
11. Kauppinen TM, Chan WY, Suh SW, Wiggins AK, Huang EJ, Swanson RA. Direct phosphorylation and regulation of poly(ADP-ribose) polymerase-1 by extracellular signal-regulated kinases 1/2. Proc Natl Acad Sci U S A. 2006; 103:7136–7141. [PubMed: 16627622]

12. Mao Z, Hine C, Tian X, Van Meter M, Au M, Vaidya A, Seluanov A, Gorbunova V. SIRT6 promotes DNA repair under stress by activating PARP1. Science. 2011; 332:1443–1446. [PubMed: 21680843]
13. d'Adda di Fagagna F, Hande MP, Tong WM, Lansdorp PM, Wang ZQ, Jackson SP. Functions of poly(ADP-ribose) polymerase in controlling telomere length and chromosomal stability. Nat Genet. 1999; 23:76–80. [PubMed: 10471503]
14. Beneke S, Cohausz O, Malanga M, Boukamp P, Althaus F, Bürkle A. Rapid regulation of telomere length is mediated by poly(ADP-ribose) polymerase-1. Nucleic Acids Res. 2008; 36:6309–6317. [PubMed: 18835851]
15. Ray Chaudhuri A, Hashimoto Y, Herrador R, Neelsen KJ, Fachinetti D, Bermejo R, Cocito A, Costanzo V, Lopes M. Topoisomerase I poisoning results in PARP-mediated replication fork reversal. Nat Struct Mol Biol. 2012; 19:417–423. [PubMed: 22388737]
16. Beneke S. Regulation of chromatin structure by poly(ADP-ribosyl)ation. Front Genet. 2012; 3:169. [PubMed: 22969794]
17. Tulin A, Spradling A. Chromatin loosening by poly(ADP)-ribose polymerase (PARP) at Drosophila puff loci. Science. 2003; 299:560–562. [PubMed: 12543974]
18. Kanai M, Hanashiro K, Kim SH, Hanai S, Boulares AH, Miwa M, Fukasawa K. Inhibition of Crm1-p53 interaction and nuclear export of p53 by poly(ADP-ribosyl) ation. Nat Cell Biol. 2007; 9:1175–1183. [PubMed: 17891139]
19. Wang Y, Kim NS, Haince JF, Kang HC, David KK, Andrabi SA, Poirier GG, Dawson VL, Dawson TM. Poly(ADP-ribose) (PAR) binding to apoptosis-inducing factor is critical for PAR polymerase-1-dependent cell death (parthanatos). Sci Signal. 2011; 4:ra20. [PubMed: 21467298]
20. Stilmann M, Hinz M, Arslan SC, Zimmer A, Schreiber V, Scheidereit C. A nuclear poly(ADP-ribose)-dependent signalosome confers DNA damage-induced IkappaB kinase activation. Mol Cell. 2009; 36:365–378. [PubMed: 19917246]
21. Bai P, Canto C, Oudart H, Brunyanszki A, Cen Y, Thomas C, Yamamoto H, Huber A, Kiss B, Houtkooper RH, Schoonjans K, Schreiber V, Sauve AA, Menissier-de Murcia J, Auwerx J. PARP-1 Inhibition Increases Mitochondrial Metabolism through SIRT1 Activation. Cell Metab. 2011; 13:461–468. [PubMed: 21459330]
22. Javle M, Curtin NJ. The role of PARP in DNA repair and its therapeutic exploitation. Br J Cancer. 2011; 105:1114–1122. [PubMed: 21989215]
23. Wahlberg E, Karlberg T, Kouznetsova E, Markova N, Macchiarulo A, Thorsell AG, Pol E, Frostell A, Ekblad T, Oncu D, Kull B, Robertson GM, Pellicciari R, Schuler H, Weigelt J. Family-wide chemical profiling and structural analysis of PARP and tankyrase inhibitors. Nat Biotechnol. 2012; 30:283–288. [PubMed: 22343925]
24. Bryant HE, Schultz N, Thomas HD, Parker KM, Flower D, Lopez E, Kyle S, Meuth M, Curtin NJ, Helleday T. Specific killing of BRCA2-deficient tumours with inhibitors of poly(ADP-ribose) polymerase. Nature. 2005; 434:913–917. [PubMed: 15829966]
25. Beneke S, Bürkle A. Poly(ADP-ribosyl)ation in mammalian ageing. Nucleic Acids Res. 2007; 35:7456–7465. [PubMed: 17913748]
26. Juarez-Salinas H, Sims JL, Jacobson MK. Poly(ADP-ribose) levels in carcinogen-treated cells. Nature. 1979; 282:740–741. [PubMed: 229416]
27. Juarez-Salinas H, Levi V, Jacobson EL, Jacobson MK. Poly(ADP-ribose) has a branched structure in vivo. J Biol Chem. 1982; 257:607–609. [PubMed: 6274856]
28. Kanai M, Miwa M, Kuchino Y, Sugimura T. Presence of branched portion in poly(adenosine diphosphate ribose) in vivo. J Biol Chem. 1982; 257:6217–6223. [PubMed: 7042708]
29. Shah GM, Poirier D, Duchaine C, Brochu G, Desnoyers S, Lagueux J, Verreault A, Hoflack JC, Kirkland JB, Poirier GG. Methods for biochemical study of poly(ADP-ribose) metabolism in vitro and in vivo. Anal Biochem. 1995; 227:1–13. [PubMed: 7668367]
30. Aboul-Ela N, Jacobson EL, Jacobson MK. Labeling methods for the study of poly- and mono(ADP-ribose) metabolism in cultured cells. Anal Biochem. 1988; 174:239–250. [PubMed: 3218735]

31. Shah GM, Kandan-Kulangara F, Montoni A, Shah RG, Brind'amour J, Vodenicharov MD, Affar el B. Approaches to detect PARP-1 activation in vivo, in situ, and in vitro. Methods Mol Biol. 2011; 780:3–34. [PubMed: 21870251]
32. Horvath EM, Zsengeller ZK, Szabo C. Quantification of PARP activity in human tissues: ex vivo assays in blood cells and immunohistochemistry in human biopsies. Methods Mol Biol. 2011; 780:267–275. [PubMed: 21870266]
33. Kawamitsu H, Hoshino H, Okada H, Miwa M, Momoi H, Sugimura T. Monoclonal antibodies to poly(adenosine diphosphate ribose) recognize different structures. Biochemistry. 1984; 23:3771–3777. [PubMed: 6206890]
34. Fahrer J, Kranaster R, Altmeyer M, Marx A, Bürkle A. Quantitative analysis of the binding affinity of poly(ADP-ribose) to specific binding proteins as a function of chain length. Nucleic acids research. 2007; 35:e143. [PubMed: 17991682]
35. Mangerich A, Knutson CG, Parry NM, Muthupalani S, Ye W, Prestwich E, Cui L, McFaline JL, Mobley M, Ge Z, Taghizadeh K, Wishnok JS, Wogan GN, Fox JG, Tannenbaum SR, Dedon PC. Infection-induced colitis in mice causes dynamic and tissue-specific changes in stress response and DNA damage leading to colon cancer. Proc Natl Acad Sci U S A. 2012; 109:E1820–1829. [PubMed: 22689960]
36. Farmer PB, Brown K, Tompkins E, Emms VL, Jones DJ, Singh R, Phillips DH. DNA adducts: mass spectrometry methods and future prospects. Toxicol Appl Pharmacol. 2005; 207:293–301. [PubMed: 15990134]
37. Wielckens K, Bredehorst R, Adamietz P, Hilz H. Protein-bound polymeric and monomeric ADP-ribose residues in hepatic tissues. Comparative analyses using a new procedure for the quantification of poly(ADP-ribose). Eur J Biochem. 1981; 117:69–74. [PubMed: 7262092]
38. Ji J, Kinders RJ, Zhang Y, Rubinstein L, Kummar S, Parchment RE, Tomaszewski JE, Doroshow JH. Modeling pharmacodynamic response to the poly(ADP-Ribose) polymerase inhibitor ABT-888 in human peripheral blood mononuclear cells. PLoS ONE. 2011; 6:e26152. [PubMed: 22028822]
39. Mangerich A, Veith S, Popp O, Fahrer J, Martello R, Bohr VA, Bürkle A. Quantitative analysis of WRN exonuclease activity by isotope dilution mass spectrometry. Mech Ageing Dev. 2012; 133:575–579. [PubMed: 22766507]
40. Beneke S, Alvarez-Gonzalez R, Bürkle A. Comparative characterisation of poly(ADP-ribose) polymerase-1 from two mammalian species with different life span. Exp Gerontol. 2000; 35:989–1002. [PubMed: 11121685]
41. Balducci E, Emanuelli M, Raffaelli N, Ruggieri S, Amici A, Magni G, Orsomando G, Polzonetti V, Natalini P. Assay methods for nicotinamide mononucleotide adenylyltransferase of wide applicability. Anal Biochem. 1995; 228:64–68. [PubMed: 8572289]
42. Beneke S, Meyer K, Holtz A, Huttner K, Bürkle A. Chromatin composition is changed by poly(ADP-ribosyl)ation during chromatin immunoprecipitation. PLoS ONE. 2012; 7:e32914. [PubMed: 22479348]
43. Wielckens K, Bredehorst R, Hilz H. Quantification of protein-bound ADP-ribosyl and (ADP-ribosyl)n residues. Methods Enzymol. 1984; 106:472–482. [PubMed: 6493065]
44. Brabeck C, Pfeiffer R, Leake A, Beneke S, Meyer R, Bürkle A. L-selegiline potentiates the cellular poly(ADP-ribosyl)ation response to ionizing radiation. J Pharmacol Exp Ther. 2003; 306:973–979. [PubMed: 12750436]

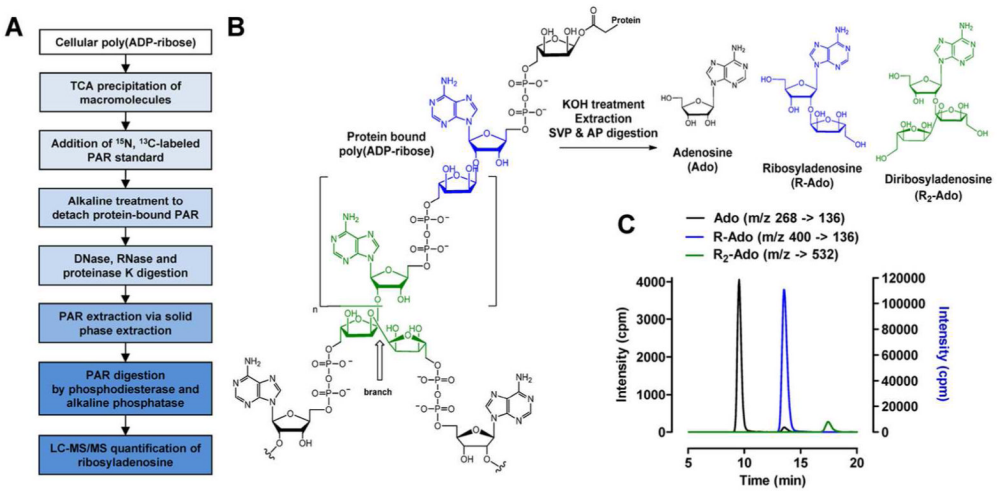


**Figure 1. Method design**

(**A**) Central steps of sample preparation for mass spectrometric quantification of R-Ado. (**B**) PAR can be quantitatively detached from acceptor proteins by alkaline treatment. Subsequent digestion of PAR with phosphodiesterase and alkaline phosphatase releases adenosine from the PAR termini and other unique nucleosides, *i.e.*, ribosyladenosine (R-Ado) and diribosyladenosine ($R_2$-Ado), which are characteristic for the linear or branched part of the polymer, respectively. (**C**) LC-MS/MS chromatogram of Ado, R-Ado and $R_2$-Ado obtained from digested PAR synthesized *in vitro*.

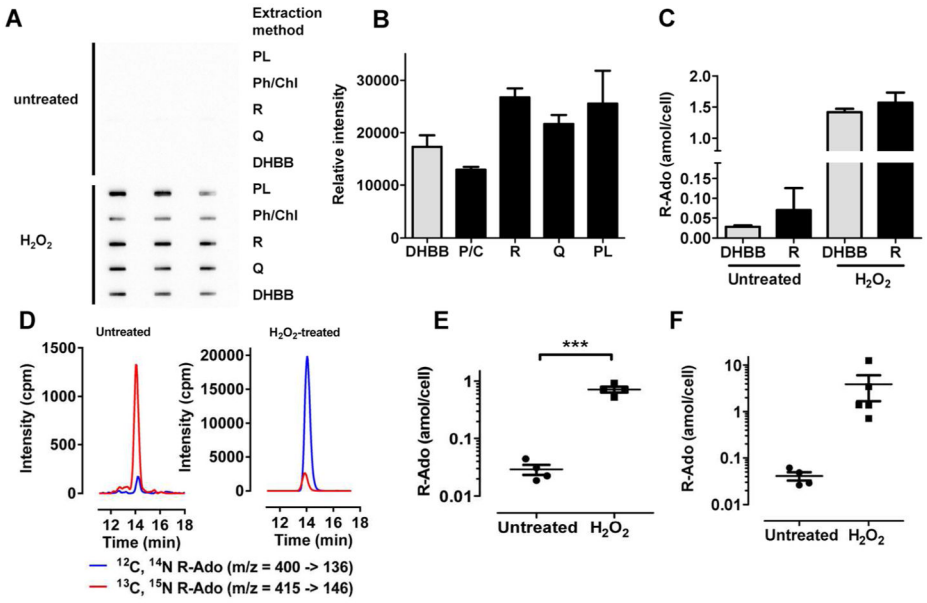


**Figure 2. Development of an LC-MS/MS-based method for the quantification of cellular PAR**

(**A**) PAR extraction from untreated or $H_2O_2$-stimulated (5 mM) COPF5 cells using phenol/chloroform (Ph/Chl) extraction, dihydroxyboryl Biorex (DHBB) affinity chromatography (DHBB), or commercially available RNA extraction kits, *i.e.*, Roche High pure microRNA isolation kit (R), PeqLab PeqGold RNA pure kit (PL), Qiagen RNeasy kit (Q). Extracted PAR samples were immobilized on a nylon membrane and detected using the PAR-specific mAB 10H. (**B**) Densitometric quantification of the slot-blot shown in (A). (**C**) LC-MS/MS quantification of cellular PAR levels extracted from COPF5 cells via classical DHBB chromatography or kit (R). Data represent means from two independent experiments. (**D**) LC-MS/MS chromatograms of cellular ribosyl-adenosine (blue) and corresponding internal standard (red) from digested PAR isolated from $1 \times 10^7$ untreated or $H_2O_2$-stimulated (100 μM) freshly isolated human PBMCs. (**E**) Evaluation of method robustness as assessed in independent experiments with PBMCs isolated from one donor (technical variability). Cells were treated with 100 μM $H_2O_2$ for 5 min. (**F**) Analysis of inter-donor variability (biological variability). PBMCs were isolated from different donors and stimulated with 100 μM $H_2O_2$ for 5 min. Data represent means ± SEM. ***$P$<0.001 (Student's t-test).

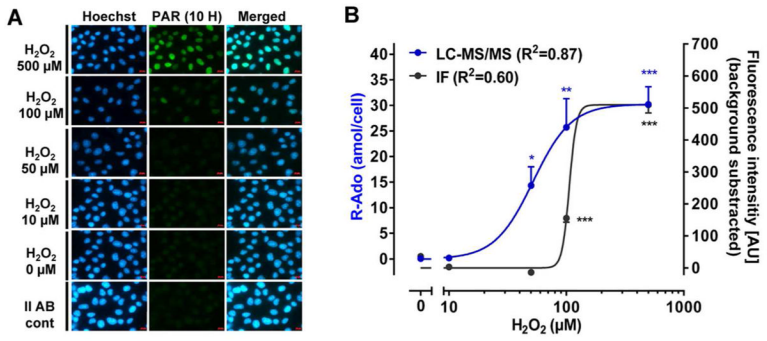


**Figure 3. Comparison of PAR quantification by immunofluorescence microscopy and LC-MS/MS in HeLa cells**

Cells were treated with increasing doses of $H_2O_2$ and PAR production was analyzed after 5 min. (**A**) Representative images from immunofluorescence-based (IF) PAR detection using the anti-PAR-specific mAB 10H. (**B**) Densitometric evaluation of IF analysis (black curve) after background substraction of secondary antibody control and LC-MS/MS quantification of PAR levels (blue curve). Data represent means ± SEM. **P*<0.05, ***P*<0.01, ****P*<0.001 (ANOVA followed by Dunnett's multiple comparison test). Curves were fitted using a sigmoidal model with variable slope.

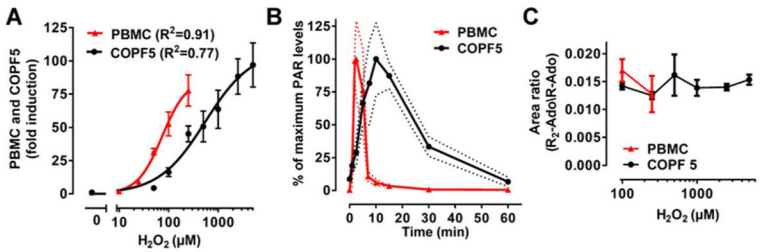


**Figure 4. DNA-damage induced dynamics of cellular PARylation**

(**A**) Dose response curves of PAR levels in COPF5 cells and PBMCs (isolated from the same donor, inter-day variability) treated with $H_2O_2$ for 5 min. Curves were fitted using a sigmoidal model with variable slope. (**B**) Time course of PAR formation in COPF5 cells and PBMCs treated with 100 μM $H_2O_2$. Data represent means ± SEM from at least three independent experiments. In each experiment PBMCs were isolated from one donor on different days. (**C**) Assessment of PAR branching by evaluation of the $R_2$-Ado/R-Ado area ratios in COPF5 cells and PBMCs upon $H_2O_2$ stimulation as indicated.

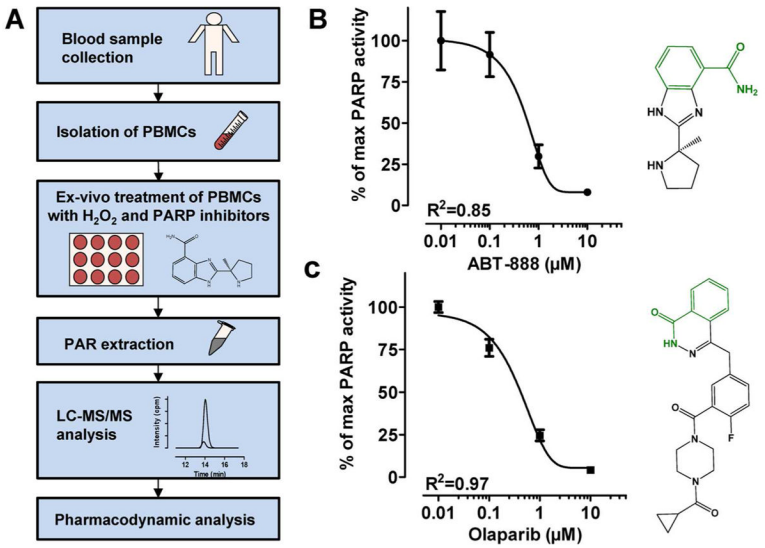


**Figure 5.** ***EX VIVO*** **pharmacodynamic analysis of PARP inhibitors**

(**A**) Method design. (**B–C**) PARP inhibition curves for ABT-888 (**B**) and olaparib (**C**) in PBMCs treated with 100 μM $H_2O_2$ for 5 min. Each experiment was performed with PBMCs isolated from a single donor, respectively, on different days (inter-day variability). Data represent means ± SEM from three independent experiments. Curves were fitted using a sigmoidal model with variable slope.

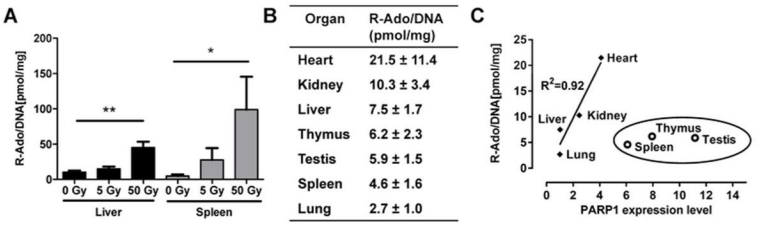


**Figure 6. Analysis of PARylation in mouse tissue**

X-ray-induced (**A**) and basal **(B**) PAR levels in mouse tissue normalized to tissue DNA content. Data represent means ± SEM from at least three independent experiments. **P*<0.05, ***P*<0.01 (Friedman test). (**C**) Correlation analysis of PAR levels and PARP1 mRNA expression levels as analyzed by RT-qPCR.